BIOMECHANICALLY REALISTIC PHYSICAL HEAD MODELS: A REVIEW AND DESIGN FRAMEWORK

Brian Michael Coyle

Box 176, Canyon, CA 94516
(925) 768-0059
bricoyle@berkeley.edu

ABSTRACT

Physical head surrogates remain essential for experimental study of traumatic brain injury (TBI), yet the headforms in current use (Hybrid III, NOCSAE, and blast-evaluation devices such as BIPED) were not designed for biofidelity. Their necks bend with directional bias and cannot represent muscle activation; their brains are homogeneous, isotropic gels; their skulls are single-material shells; and cerebrospinal fluid, when present at all, is crudely approximated. This review synthesizes recent findings in injury biomechanics and soft-materials science to argue that substantially more realistic head models are now achievable at low cost. Evidence from athlete and volunteer studies shows that neck muscle activation, mediated largely by visual anticipation of impact, reduces rotational head acceleration by roughly 20–25%, so surrogate neck stiffness should be configurable by impact direction relative to the visual field. White matter deforms anisotropically along axonal tract directions, a property isotropic silicone simulants cannot capture; newly developed hydrogels, aligned by magnetic fields, shear, light-templated assembly, or freeze casting, reproduce direction-dependent moduli comparable to white matter, and ultrasoft siloxanes match gray matter. Multi-material casting and 3D printing with soluble molds permit assembly of gray- and white-matter analogs with the realistic interfaces where strain concentrates and injury localizes; the composite brain model developed from this approach has issued as U.S. Patent 12,784,616, and the section on brains describes its design. For the skull, PLA-family composites approximate skull bone bending moduli, and layered printing can reproduce the cortical–diploë–cortical sandwich. The review concludes with a design framework for an affordable, biofidelic, partly recyclable surrogate head for angular impact and blast testing, instrumented with a patented sensor that measures rotational displacement directly.

Key terms — Traumatic brain injury; physical head surrogate; biofidelity; anisotropic hydrogels; skull mechanics; cerebrospinal fluid; rotational acceleration.

1. INTRODUCTION

Experimental study of TBI faces a basic dilemma. Animal models raise ethical concerns and involve brains whose geometry, scale, and material organization differ substantially from human brains.

Cadaver tissue loses the mechanical properties of living tissue: muscle tone decays, trabecular bone fillings degrade, and brain tissue dehydrates and stiffens or softens unpredictably after death. Finite element (FE) simulation has advanced considerably, but FE models of localized axonal injury have often gone unvalidated against physical experiments, and rotational acceleration, the loading mode most strongly associated with diffuse axonal injury, has proven especially difficult to simulate. Physical head surrogates therefore remain indispensable: they can be instrumented, subjected to repeatable impacts and blasts, and used to validate the FE models that increasingly guide helmet design, vehicle safety standards, and blast-protection equipment.

The problem is that the surrogates in standard use were never designed to be biofidelic. The Hybrid III neckform, built from alternating metal and butyl rubber discs, is biased toward sagittal bending and responds to angular impacts with significantly slower rotational acceleration than alternative neckforms. No standard neckform represents musculature at all, despite evidence that muscle material properties can alter tissue stress and strain by up to 70%, and despite consistent findings, from instrumented hockey players, ball-drop experiments, and sled tests, that anticipatory muscle activation measurably reduces rotational head acceleration. Standard surrogate brains are homogeneous, isotropic silicone gels such as Sylgard 527, whose decay constants differ from brain tissue by orders of magnitude and which cannot represent the defining mechanical feature of white matter: anisotropic deformation along aligned axonal tracts, the best available predictor of mild TBI in National Football League impact data. Alshareef et al. selected Sylgard 527 as the brain simulant for a 3D biofidelic head surrogate, choosing it from six gels evaluated by shear rheometry, and measured intracranial deformation by MRI and sonomicrometry [1]. That work shares this review’s premise, that physical surrogates used for equipment evaluation lack internal measures of brain deformation and that greater biofidelity is needed. However all six of their candidate gels were isotropic, so the comparison identified the best isotropic simulant but could not test an anisotropic one. Shear rheometry characterizes at rates far below impact, where the rate-dependent inversion described in Section 3.3 applies. The anisotropic hydrogels reviewed here were not available as candidates in that comparison.

Surrogate skulls are typically single-material shells of aluminum, polyethylene, or polyurethane, without the cortical–trabecular sandwich structure that gives real skull bone its combination of stiffness, cushioning, and bending strength. Cerebrospinal fluid is usually omitted, although a simple 2 mm water layer has been shown to reduce maximum shear strain in a surrogate brain nearly threefold.

This review argues that the materials and fabrication methods needed to close these gaps now exist, and that most are inexpensive. Its contribution is to connect two literatures that have developed largely in isolation, injury biomechanics, which has documented what a biofidelic head model must do, and soft-materials science, which has recently produced hydrogels and elastomers that can do it, and to present the author's patented composite brain model [2] as an implementation of that connection. Anisotropic

hydrogels, aligned by magnetic fields, electrical fields, shear, light-templated nanostructure assembly, or freeze casting, now exhibit direction-dependent shear and tensile properties in the range of white matter. Ultrasoft polysiloxane elastomers match gray matter moduli. Multi-material molding and 3D printing with water-soluble molds permit these materials to be cast in anatomically realistic configurations, preserving the gray/white interfaces where mechanical mismatch concentrates strain and injury. Consumer-grade printing polymers, PLA and its blends, approximate skull bone flexural properties, and layered printing can mimic the skull's sandwich construction. Membrane-enclosed fluid layers can do this for CSF.

The review proceeds anatomically. Section 2 examines the neck, including the role of muscle activation and impact anticipation, and proposes direction-dependent neck stiffness as a design principle. Section 3 examines the brain, contrasting the isotropic silicones favored in blast research with the anisotropic hydrogels emerging from biomedical materials research, and describes fabrication methods for composite, heterogeneous gray/white models. Section 4 examines the skull and evaluates printable materials against cadaver bone data. Section 5 addresses cerebrospinal fluid, and Section 6 surveys instrumentation. Throughout, the emphasis is on materials and methods that are affordable and rapid enough that surrogate components can be treated as consumable, sacrificed in testing, which is what routine experimental use requires.

Current helmet impact testing protocols are based on the most frequent instantaneous impact forces athletes experience, from accelerometer data in athletic helmets. Without baseline data about brain tissue response to a wide variety of impact scenarios, a helmet system cannot be evaluated for reducing impact response that may cause brain tissue damage.

2. THE NECK

A realistic head model sits on a realistic neck. Muscles are not static structures like bones and brains. Muscles contract and relax, sometimes reflexively, often due to voluntary effort. Neck muscles play a critical role in head movements. Evidence motivates a design principle developed below: surrogate neck stiffness should be configurable according to impact direction relative to the visual field resulting from head orientation.

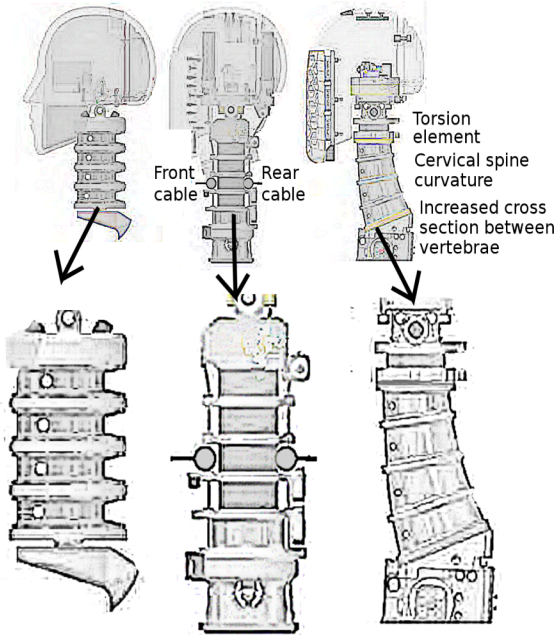


Figure 1 Drawn by author

2.1 SURROGATE NECKS

Hybrid III neck models used in crash, blast and helmet tests use four or five metal discs interconnected by four incompressible butyl rubber
discs. A single fissure in the rubber reduces neck stiffness. This, however, biases the neckform to bend directly backwards and forwards, a biased response for impact testing. Such necks showed significantly slower rotational acceleration from angular impacts compared to a NOCSAE neckform [3].

Wayne State's THOR neck model uses six metal discs and twelve silicone foam rubber rings to simulate intervertebral disks. Its design simulates ligaments and musculature, as well as vertebrae, with multi-axis joints. This better represents rotational dynamics caused by oblique impacts. Humanetics Inc., affiliated with Wayne State, developed a more sophisticated (neck and head) dummy called THOR-AV. It has greater structural biofidelity, incorporating neck curvature, with vertebrae offset at different distances and angles.

Physical principles imply that shorter, thicker necks will respond more stiffly to angular impacts. For a vertical mass, a larger diameter increases I, the second moment of area (proportional to r^4, where r is radius) $I = \pi r^4 / 4$. Shorter, thicker columns resist buckling under compressive or angled loads. In Euler's buckling formula the critical force $F_{critical} = \pi^2 E I / (KL)^2$ where E is modulus, L is height, and K is how supported the column is. This is analogous to the logic that athletes with shorter, thicker necks resist angular impacts better than people with thinner, longer necks. However, there is an important factor in humans that such models do not incorporate: real neck response to impacts is governed by muscle activity as much as muscle area.

Humm et al. compared the Hybrid III and Thor systems with cadavers, and found Thor systems were somewhat more accurate in representing actual injury under impact accelerations found in vehicle crashes [4]. Wang et al. crashed the three different systems at angles (oblique impacts) to see how well their neck movements compared to real human necks during collisions. Several different testing devices were used. Overall, THOR-AV was marginal to good, THOR marginal, and Hybrid III poor, in terms of human-like rotation responses. None allow attached heads to twist sideways like real people do in angled crashes. The THOR-AV actually spun too much in some of the tests, presumably because of a special rotating part in its design [5].

The greater biofidelity of THOR systems may be due to the arrangements of component structures. For example, Awad et al.'s 2015 paper assessed a modified THOR neck, along with brain, skull, and skin components. The neck incorporated 6 steel discs, with silicone foam rubber rings on either side of each. From the top, 4 steel cables were run to each of 4 steel disks. The cable ends were attached to springs, either to one of 4 springs, or cables grouped to fewer or all at a single spring. The authors compared neck flexion and found using one spring per cable (which they compared to neck tendons) mimicked

human neck flexion best, 15° - 30° [6]. Flexion and extension of the neck refer to back and forth movements. The authors did not report rotational movement. Bogduk & Mercer reviewed human neck structural motion. In seven studies flexural motion ranged from 10° to 21°. In normal individuals neck axial rotation from CT scans averaged 43° to either side [7].

Neck model materials may not be biofidelic. In humans, cervical vertebra are not flat disks. The top disks, which are critical for head motion, have highly convex shapes formed by thick cartilage tissue. The first disk (the atlas) moves down into the second disk (the axis) during head rotations. The atlas and head rotate from side to side as one unit. Other cervical vertebrae respond to different impacts in complex ways, often with some having the reverse motion of others [8].

Cadaver tests find that the effective modulus of human intervertebral discs ranges from ~5 to 50 MPa [9]. Hybrid III uses butyl rubber discs. Different butyl rubber suppliers report variable modulus rates, but these include the range of human tissue. THOR systems' silicone foam rubber has a lower Young's modulus than human discs, below 5 MPa.

Neither Hybrid III, Thor, nor other neckforms use biomimetic materials for neck muscles. Differences in muscle material properties can change tissue stress and strain by up to 70%. There's little data on the mechanical properties of such muscles. Arnold, Scott & Bush reviewed, in 2023, studies of soft tissue mechanical properties of humans, including muscles. No study focused on neck muscles. Overall, *in vivo* studies of muscles report higher Young's modulus than cadavers. This isn't surprising, since muscle tone presumably weakens without metabolic inputs or exercise [10].

2.2 PREPARATORY MUSCLE ACTIVATION

Harry Houdini withstood countless expected blows to the abdomen; a single unexpected one injured him seriously [11]. It highlights how preparatory muscle activation ahead of an expected perturbation is a whole-body, feedforward process.

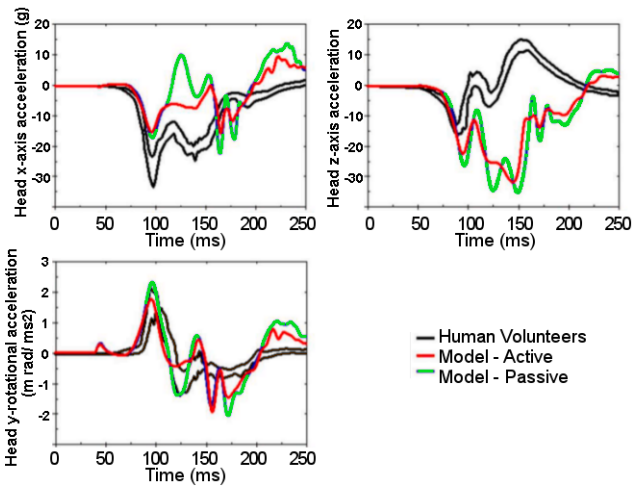


Figure 2 Redrawn from Nightingale et al. [12]

Cadavers (and current model necks) cannot activate muscles. Muscle activation is important in resisting head movements after impacts. Computer models suggest muscle activation plays an important role in responding to impacts that induce head movement [12]. Nasim & Galvanetto assembled a complex FE neck model that incorporated various muscles, and ran a simulation under 15g frontal impact loading. This was compared to similar data of young male volunteers engaged in sled tests. Two FE models were used, one with muscles activated during impact,

and one with muscles passive. The FE active muscle model was somewhat better at predicting subject responses. The experimental data showed that active muscles of the lower neck play an important role in response to impact forces. Muscle activation increases neck strength to resist head motion.[13]

The difference between both FE models and experimental evidence was large. Fig. 2 shows 15g frontal impacts, with passive and active neck models compared to volunteer experiments, from Nightingale et al. FE models exaggerated acceleration in the X-axis, failed to predict Z-axis acceleration, and modestly correlated with volunteer response in the Y-axis.

Evidence about neck muscle strength and increased neck stability during impacts is mixed. Neck muscle strength training for eight weeks did not enhance head-neck stabilization during force application in collegiate soccer players [14]. But evidence for muscle activation and reduced head movement is abundant. Although activation may be reflexive, it often requires a person's awareness of an imminent impact. Awareness helps to protect, being struck without expectation is more damaging.

The key neck muscles in neck stabilization are the sternocleidomastoid (SCM) and trapezius muscles. They help control head–neck flexion and extension. Ito et al. found that reflexive response of the SCM begins to decelerate head velocity before voluntary movement takes effect [15]. Bauer et al. monitored activity of the left and right SCM and trapezius muscles with electrodes attached to player's skins, over the muscles. They analyzed muscle activation during heading. The SCM became active earlier than the trapezius and showed greater activity before ball contact. The trapezius became active just before ball contact and showed greater activity after ball contact. The combination stabilized the head-neck complex [16].

Muscle activation is only partly reflexive; athletes activate muscles differently depending on their expectation of impacts. Kumar et al. seated subjects in chairs, and these chairs were impacted with a pneumatic device that caused sudden movement at speeds of about 4.5 to 11 m/s, then were abruptly stopped. Subjects were either informed of the impending impact, or blindfolded. Peak shoulder and head acceleration was more significantly correlated with whether the impact was expected, than with muscle mass or gender [17]. Tierney et al. put electrodes on SCM and trapezius muscles on 40 subjects, who were seated and had a 1 kg ball dropped 15 cm on their heads. Subjects were either warned 3 seconds prior a ball drop, or told that sometime in the next 30 seconds a ball would drop. Males had 25% less rotational acceleration when expecting the ball drop. Females did not differ between the two conditions, but may have been more vigilant in both [18].

A real-world study of impact anticipation and muscle activation showed it had an effect for medium-intensity impacts. Mihalik et al. placed HITS accelerometers in helmets of 16 male hockey players aged 14, and videotaped the players for 54 games. 666 collisions were both detected and observed. The authors determined whether players anticipated impacts or not. For the most severe linear and

rotational acceleration-causing impacts, anticipation did not matter. But in medium-intensity impacts there was a significant, 20% reduction in rotational acceleration when the impact was anticipated. Anticipation meant the athlete saw the collision coming. The authors hypothesize that when an impact is anticipated, cervical musculature is contracted, and the head accelerates less [19].

Mihalik et al.'s results resemble what is found in results of freefall in humans. A person who falls responds with rapid neck and limb activation, and the response is protective. As fall height increases, however, the same activation contributes proportionally less, and beyond some height it serves no protective purpose, and may become counterproductive [20]. A braced limb transmits load rather than absorbing it, which is why parachutists and stunt performers are trained to land loose. The same logic may apply to the neck. If in response to severe loads cervical activation still resists some head motion, it transmits load. Whether this causes greater brain rotational acceleration than a neck overwhelmed by an impact that causes the head to rotate rapidly is an open question. Resolving it requires an instrument that reports regional tissue response rather than headform kinematics.

Another combination telemetry and video study, this one of American high school football players, found player stance most correlated with concussion. The authors tried to determine if players were looking in the direction of collision, but rater reliability was low and anticipation level absent [21].

Anticipation generally requires visual sighting of the entity that will be collided with. Visual fixation or tracking is closely associated with neck muscle activity. Coordination between eye and neck movement is important in posture stability, especially during impacts that can cause head movements [22]. The link between visual stimulus and neck muscles is tight. Research with monkeys showed that visual cues induced neck muscle activity before further eye movement occurred [23]. However, periods of extreme muscle activity reduce neuromuscular control of the body. Neck muscle activation should remain reduced unless impacts are expected [24].

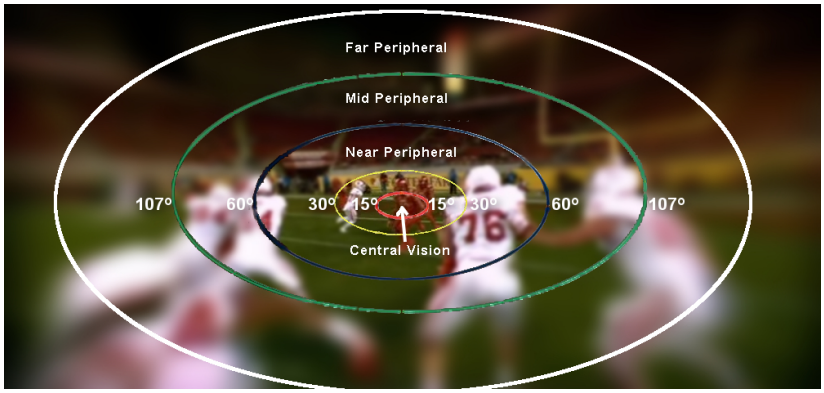


Figure 3 Redrawn from Younis et al. [26] with author's photo

People respond to cues more slowly, and with less accuracy, to visual stimulus in their peripheral vision, problems that significantly increase with the degree of peripherality. Impacts that approach in

the visual periphery, or from outside the visual field, are associated with slower muscle activation [25].This is illustrated in Figure 3 [26].

Contemporary large football helmets reduce player peripheral vision, and a study found this impaired player reaction time to peripheral visual stimuli. The authors suggested larger helmets and eye shields intended to mitigate head impacts may have the unanticipated consequences of decreasing player safety and performance. Enhanced peripheral vision acuity reduces reaction time and accelerates target detection; diminished peripheral acuity correlated with slower response to lateral targets [27].

15 high school male hockey athletes were put through oculomotor tasks, tracking rapidly moving and peripheral objects. They were scored by oculomotor performance. During the following competitive ice hockey season, players with higher oculomotor scores had fewer head impacts; players with less efficient oculomotor performance were associated with increased incidence of head impacts [28].

Clark et al. reported that in U.S. high school soccer athletic population, female athletes incur a higher concussion rate than males. No consensus has been established to explain this high incidence rate, but many mechanisms are proposed, including cervical spinal musculature, skull thickness, hair length, and psychological factors. Women are assumed to report injuries more than men. Heading the soccer ball is one of the primary conditions that lead to player-to-player head contact in soccer, and many young players close their eyes during heading. The authors analyzed photographs of high school players heading soccer balls, and found women were more likely than men to have eyes closed. This correlation with higher injury suggests visual anticipation reduces concussion risk [29].

2.3 GUIDANCE

A neck model is optimized by having increased flexibility for impacts from directions in a model head's axial periphery or outside its predicted view field. Neck models are usually configured as if for active muscle condition, accurate for impacts within the core visual field. **As impacts are programmed to come from more peripheral directions, the configuration can be modified for increased flexibility, with head movement increasing**. When testing helmets, the range of potential vision can be determined, and neck flexibility modified for specific impact directions that correspond to targets that may or may not be seen. For example, the Hybrid neck model has a nut that can be loosened to raise the head, increasing the neck's flexibility.

A biofidelic neckform, then, is not one with fixed properties, but one whose stiffness varies with the modeled direction of impact awareness.

3. THE BRAIN

The critical challenge for a surrogate brain is that brain tissue is not one material. Gray and white matter differ in composition, mechanical behavior, and, most critically for rotational injury, in their directional response to load. This section reviews the mechanics a surrogate must reproduce, the silicone simulants developed in blast research and the two limits they have reached, the anisotropic hydrogels emerging from biomedical materials research that can pass those limits, the complication of loading-rate dependence, and fabrication routes for assembling composite gray/white models.

3.1 MECHANICAL BEHAVIOR OF GRAY AND WHITE MATTER

Gray matter consists largely of neuronal cell bodies, dendrites, non-aligned local axons, and synapses, supported by glial cells and capillaries; because these elements have no dominant orientation, gray matter is mechanically isotropic. White matter consists of aligned axonal fibers and is considered anisotropic [30]. White matter is composed predominantly of long-distance myelinated axons organized into tracts running in defined directions, transporting information for inter-brain coordinated activity. The white color is due to white myelin protecting these axons.

White matter has been further divided into groups based on the alignment of these fibers. For example, the superior longitudinal fasciculus connects frontal lobes to parietal and occipital lobes at the rear of the brain. Its axon tracts are aligned horizontally, from front to back. The corticospinal tract axons run from the brain to spinal cord, its fibers aligned vertically. The uncinate fasciculus involves long axon fibers that bend from the orbital frontal cortex around to the anterior temporal lobe and back to the amygdala. Brain tissue deformation has consistently been shown to occur when white matter axon tracts are strained along their alignment direction [31].

This alignment makes white matter anisotropic: tissue deformation occurs lengthwise, whereas loads perpendicular to a tract compress fibers without comparable risk of failure. TBI is associated with anisotropic response of axonal fibers. As impacts extend a fiber along its pathway it thins, and if bent or twisted fibers can fail. The clinical relevance is direct. For a data set of mild TBI from the National Football League, strain in the axonal direction was found to be a better injury predictor than maximum strain, averaged strain, or cumulative strain [32].

Axonal-strain models have been questioned on the grounds of interindividual variation in tract geometry. Alignment orientation, and the degree of strain they may suffer, varies between individuals. Veenith et al. found the SLF and corticospinal tracts had around a 3.5% interindividual variance, the uncinate fasciculus a 6.0% variance [33]. Another study, using white matter axonal tract patterns of 485 subjects aged 22–35 years, modeled their predicted strain. This found a coefficient of variation between

subjects of nearly 12% for maximum axonal strain. In that study, however, the locations of maximum axonal strain did not vary between subject [34].

There are consistent patterns of gray and white matter regions within primate species, including humans [35]. Gray and white matter volume, cortical area, and architecture are similar among primate populations. Variation in the fine-grained level of the depth or shape of brain foldings may occur between subjects, but not overall structural organization [36]. The parts of human brains that vary least in relative size are gray areas with the most white matter connections to other parts of the brain [37].

For surrogate design this is the salient result: a physical model is an approximation, but the anisotropic regions that concentrate impact strain are consistently located, along with the isotropic gray matter regions that resist it. Areas where gray and white matter have extensive surface contact are where impact-related biomechanical interactions occur [38]. Under rotational acceleration, softer gray matter drags stiffer white matter, imposing greater tensile elongation on axons near interfaces than in white matter regions more isolated from gray. Mechanical mismatch of this kind can take up to centimeters to reach equilibrium, increasing white matter anisotropic strain and leading to material damage over that distance. A surrogate brain that homogenizes the two tissues therefore erases precisely the regions where injury localizes.

The angular momentum of a brain around its mass center imposes strain between white and gray matter due to their different biomechanical responses. Strain concentrations occur at their interfaces. From a purely physical perspective, the main factors that govern strain propagation at an interface between two materials is the degree of mismatch in the elastic properties of the materials [39]. Computation models predict that gray-white matter interfaces, which axons intersect and where each matter has mechanical differences, impose amplified stress on axons. The long, thin architecture of axons, bundled in extensive organized tracts, and their viscoelastic nature, increases damage from shear and tensile forces as the brain is rapidly deformed [40]. More severe local injury occurs near white and gray matter boundaries. In one example, the corpus callosum followed the skull's motion more closely than more compliant gray matter that readily deforms around it, straining axonic connections [41].

The fractional anisotropy of several brain regions, from diffusion tensor imaging, was estimated (Table 1).

TABLE 1. Fractional anisotropy (DTI) of brain regions [42].

Brain region	**Fractional anisotropy**
Occipital lobes (gray)	0.0–0.2
Frontal, parietal lobes (gray & white)	0.2–0.3
Thalamus (gray)	0.3–0.4
Corona radiata (white)	0.4–0.6
Corpus callosum (white)	0.6–0.9

The most significant difference in anisotropy in brain areas is between gray and white matter [42].

Chan et al. placed subjects 33 male and female subjects in an MRI machine with a head cradle. Subject heads were mildly rotated using the cradle, repeated up to 52 times for 13 images at successive tissue depths. This imaged most of each brain during rotations. The rate of head motion was ~200 rad/s2, only 10-15% of the angular accelerations experienced by soccer players heading a ball. They superimposed grid patterns onto brain tissue, each voxel in the grid moving with the tissue as it deformed. For each voxel they calculated a displacement vector that showed how far and in what direction it moved. A Lagrangian strain tensor was applied to voxels grouped by brain tissue, to show how tissue stretched, compressed, or sheared. The maximum shear strain measured the maximum amount of deformation that occurred when tissue materials slid past each other while remaining in contact. Cortical gray matter strains were highest, followed by white matter (much of it directly below the outer cortex) followed by deeper gray matter. Cortical gray matter changed shape more than the white matter it covers, which changed shape more than gray matter embedded in it [43].

As will be seen, blast studies with physical models generally use silicones as artificial brain materials. Medical studies with physical brain models often use hydrogels. Silicones are stiffer than hydrogels; superficially, this aspect makes the former resemble white matter and the latter gray. But there are other important variables, the most important of which is their behavior when suddenly loaded. In the past both silicones and hydrogels responded isotropically. It is critical that any material representing white matter respond anisotropically, in particular stressing in the direction of impact. This is the condition that causes axons to deform.

Contemporary silicones can be made as soft as hydrogels, but they remain isotropic. On the other hand, hydrogels have been developed that respond anisotropically in ways that mimic white matter. Silicones are isotropic; hydrogels can exhibit anisotropy.

3.2 BLAST STUDIES, SILICONES AND SILOXANES

Because of the many service members with TBI from Improvised Explosive Devices (IEDs), researchers have examined the effects of powerful blasts on brains. Head forms with model brains are placed in shock tubes. Analysis is made of powerful blast waves on the brain models.

Blast studies converged on silicone gels as the optimal material for brains. Further, different silicone formulations may represent different brain materials. Wayne State University has developed brain injury models since the 1960s. In the post 9/11 period they focus on blast impacts.

In a 2010 University of Nebraska, Lincoln thesis, Hossain prepared different experimental models of human heads incorporating model brains. Materials simulating skin, skull and brain were tested. The

brain material tested included water gels, oil based compounds, and silicone gels. Their viscoelastic properties were tested under different stress levels. Silicone gel had the most promising results for brain models. Because silicone dynamic modulus was higher than human brains, thinner was added to soften it up. Gelled in a mold with accurate geometry, the author put the brain in an artificial skull, covered in simulated skin, then made preliminary blast tests on the model [44].

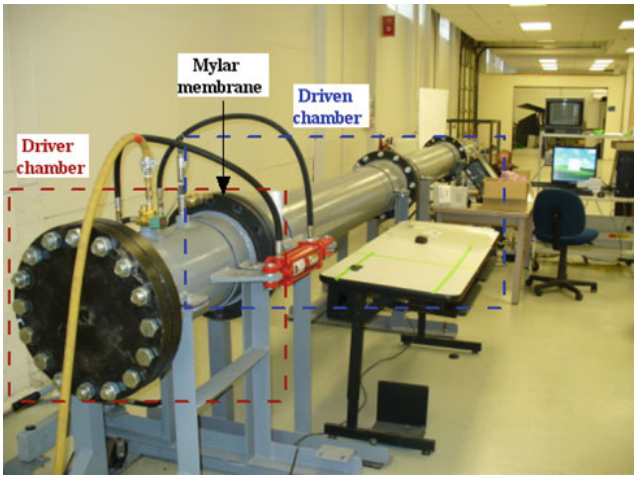


Figure 4 Shock Tube System at Wayne State, from Zhang [45] shared under CC BY 4.0

The author's conclusion was that for brain simulant material in blast tests, appropriately thinned silicone gels are better than water-based gels or oil-based compounds.

Surrogate brains in head forms can record rotational data that FE simulations can have difficulty predicting. In a 2012 paper Zhu et al., at Wayne State, reviewed research, and carried out their own, on blast-induced TBI [46]. Animal experiments required great effort to conduct experiments, and even more resources to examine resulting biological tissues. This limited the number and scale of these studies. The authors found that FE simulations had found localized stress-caused axon injuries, but none were validated against experimental data.

The authors made a physical head surrogate, then based an FE model on experimental results. The FE tests were validated with more head experiments. The surrogate was an egg-shaped deformable object. The simplified geometry reduced the FE complexity. A more realistic head with a multilayered skull and inhomogeneous brain tissues was too difficult to computationally model and interpret.

The surrogate skull was a polyethylene shell; the brain was a silicone gel brain simulant, Sylgard 527 A&B (Dow Corning.) Sylgard's mechanical properties, under strain, are reported to be similar to those of brain tissues during car crashes. A fiber optic sensor in the brain recorded internal pressure. The FE model was modestly validated with surrogate results, but even the simplified surrogate generated more complexity than the FE could process. This was despite the single blast being more or less uniformly distributed over the surrogate's frontal surface, and the homogeneity of surrogate materials.

The authors did examine how the surrogate's orientation altered pressure responses, and FE predictions. They turned the surrogate so blast waves struck it off-axis, but fixed the surrogate in place. Otherwise the blast would rotate it. Although the surrogate could record rotational data, the FE model did not have the capacity to simulate rotational acceleration. Physical surrogates, in other words, are not merely validation targets for simulation; they capture responses simulation cannot yet reach.

Zhu et al. reported the following material properties of their Sylgard 527 silicone gel brain model, and I compare these to typical material properties of real brains (bovine, porcine, and human.) Values vary according to age, anatomical region, temperature, etc. Table 2 presents the comparison.

TABLE 2. Material properties of the Sylgard 527 silicone gel brain surrogate of Zhu et al. [46] compared with averaged values for brain tissue.

Property	**Sylgard silicone gel**	**Brain (averaged)**
Density	950 kg/m³	~1040–1060 kg/m³
Bulk modulus	1.0 GPa	2.1 GPa
Short-term shear modulus	3,600 Pa	~1500–3000 Pa
Long-term shear modulus	586 Pa	~100–500 Pa
Decay constant [47]	0.05 ms	~10–100 ms

Most properties are within striking distance, as density and shear moduli are of the right order, but the decay constants differ by roughly three orders of magnitude. The large difference between the Sylgard and brain decay constants is problematic, because decay times are associated with injury-level brain deformation: non-lethal, sports-related shear injury involves motion that is far from instantaneous. Nicolle et al.'s study of shear on porcine brains, from which the decay constant data above is drawn, recorded from 10^{-5} s to 270 s, although based on linear head acceleration only [48]. Hrapko et al. found that friction between a porcine brain and the plate on which it is positioned had a significant effect on shear measurements over time. Friction between the brain and its supporting surface significantly and linearly modifies shear decay over time. This is an important consideration, because a brain's tethering within the head produces exactly such friction, and modifies decay of movement over time [49].

In a 2018 paper Chanda et al. addressed the significantly different biomechanical properties of the cerebrum's white and gray matter. The authors recognized that white and gray matter must be distinguished in any brain injury test, including blast studies. Such data cannot be recovered in cadaver tests, where brains have mechanical behavior changes due to tissue dehydration and death. The authors developed patented silicone-based materials that mimic some of the mechanical behavior of gray and white matter tissues. They began with five different silicone ratio blends, each with different stress and strain rates. The softest silicone simulation material corresponded to gray matter properties, and the hardest material corresponded to white matter. The nonlinear stress versus stretch responses of the

brain tissue surrogates were characterized by different models, and Yeoh's hyperelastic model, which models incompressible materials like rubber most accurately, predicted the behavior of both. Chanda et al. developed silicone blends at five mixing ratios spanning gray-matter-like (softest) to white-matter-like (hardest) stress–strain response, characterized by Yeoh's hyperelastic model [32]. But the authors themselves note their limitation: the materials are isotropic and therefore do not model angular loading [50].

The silicones are low-cost, and can be used for experiments and practicing surgeries. However they respond isotropically to loads. Under uniaxial tension in blast tests, this may be realistic. But helmeted collisions in sports cause angular forces, which cause anisotropic, not isotropic, brain effects. The authors do not report decay constants, which may be similar to Sylgard [51].

Chanda et al. filed and obtained a patent for crosslinked siloxanes, a type of silicone material, that exhibit "non-linear" behavior: the material's stiffness changes as it is loaded or deformed. It may go into plastic deformation after a certain stress level. Mammal skins are nonlinear-elastic material, which promotes tear resistance [52]. Chanda et al.'s patent described siloxanes that mimic human skin, in particular vaginal skin [53]. In a later paper reviewing the siloxanes they had developed, the authors noted the limitation that these materials, being isotropic, do not model angular forces well [50].

Gray matter is soft. Gray matter under load has a 1 to 1.4 kPa modulus [54]. Silicones, in the past, were not particularly soft. However Chanda et al. and other researchers have found siloxane elastomers that are very soft, by varying the crosslink density of elastomers. Vatankhah-Varnosfaderani et al. developed polysiloxane elastomers with multiple, covalently-linked side chains that have Young’s moduli below 1.2 kPa. The ultrasoft moldable elastomers expand extend isotropically. Material like this is suited for models of gray matter, though not white [55].

3.3 BRAIN MODELS FOR MEDICAL RESEARCH AND HYDROGELS

A largely separate literature, involving medical modeling and tissue engineering, has favored hydrogels. A number of researchers have used hydrogels in models of whole brains, without differentiating white and gray matter. Like brain, hydrogels are mostly water (biological soft tissues are 50–85% water by weight), and their mechanics are tunable through composition. Whole-brain hydrogel models have reproduced properties silicones do not attempt. Ray et al. sought a method to assess particle movement through brains. They started with on MRI scans, from which they designed, in CAD, the outer pial surface of a brain in a mesh surface. This was 3D printed, and a mold was made from it. 0.6% agarose was inserted into the mold, gelled, then removed. Agarose forms a porous hydrogel that allows molecules to migrate through it. The gelled brain produced an anatomically accurate cortical surface with gyri, the folded structures raised on the cerebral cortex, and sulci, the furrows between them. Such a structurally accurate model of the visible shape of the brain cost less

than $100 in materials. When used to test different particle diffusion models, the geometric fidelity measurably improved predictions of particle transport compared with a plain gel block [56]

Formal models of brains tend to be either poroelastic or viscoelastic. A 0.6% agarose gel mimics the poroelastic brain properties. Poroelasticity describes porous semi-solid matrices saturated with fluid flows. Stress and strain in the porous material affect fluid pressure. Poroelastic models are best for studying the interaction of fluids and tissue. Viscoelastic models, instead, are best for studying tissue under loads. A brain's viscoelastic material parameters may predict the response of brain tissue under uniaxial and multiaxial loading conditions. Viscoelastic properties are examined in blast tests.

Composite hydrogels have matched viscoelastic response as well. A composite hydrogel consisting of a rigid polysaccharide network (sodium alginate and pectin) and a flexible polyacrylamide network, exhibited brain tissue-like mechanical properties under various solution environments and strain rates. The hydrogel brain model behaved similarly to a porcine brain under different loading conditions. The intrinsic shear modulus of the hydrogel and brain tissues were similar, the material again costing under $100. [57] Hydrogels made with agarose and acrylamide can be prepared in concentrations other than 0.6%. This changes their viscosity. Composite structures made with hydrogels having different viscosities may better represent different types of brain tissues, and show both poroelastic and viscoelastic response to nonlinear impacts [58].

Kainz et al. synthesized a hydrogel with polyvinyl alcohol and Phytagel that mimicked a porcine brain, and examined its viscoelastic properties. The hydrogel was able to match several material responses, including a porcine brain's characteristic relaxation rate, its adhesive behavior, and structural features resulting from a brain's porous nature [59]. The same authors later provided a computational analysis, based on a cadaver brain, that modeled the brain as a combined poro-viscoelastic material. They found that that gray and white matter had different viscous and porous effects. This explained large variations in measured properties of brains that did not differentiate between them. At small, common loading rates, more fluid flows through white matter, and gets squeezed out of it, than in gray matter. Under these loading conditions, white matter appears softer than gray. But at fast loading rates, such as in collisions, white matter stiffens as fluid is trapped in it, becoming stiffer than gray matter [60].

Compared to complex brain tissues, hydrogels are simple structures. Biological soft tissues serve as a medium for dynamic biological processes. At the same time they have elaborate structures, with multiple components in hierarchies from molecular to macroscopic scales. This combination of squishiness and structure permits sophisticated functions to evolve. Hydrogels are squishy, but in the past, like silicones, there were isotropic structures. Driven by tissue-engineering applications, as many metazoan tissues are anisotropic from molecular to macroscopic scale, materials researchers have now developed several fabrication routes that align internal structure during gelation, yielding direction-

dependent mechanics [61]. With hydrogels often explored as scaffolds for dynamic living tissues, numerous efforts try to fabricate anisotropic gels that can move accordingly. This usually requires managing hydrogel synthesis with some type of external force. Such hydrogels contain components that can be directed into position with external stimuli, such as mechanical forces, magnetic and electric fields, and gradients of temperature and ions [62].

Shear forces can be applied to orient nanofibers and nanofillers during their situ polymerization in a dispersion. Manually applied shear forces tend to vary inconsistently. Dispersions with electrical nanofillers can be electrically oriented, often into thin hydrogel films. These require care in the arrangements of electrical contacts, to avoid electrochemical decomposition. Magnetic nanofillers form anisotropic hydrogels under applied magnetic fields. Magnetic forces are applied in a noncontact, nondestructive, consistent manner, and penetrate homogeneously into samples. This can synthesize anisotropic hydrogels with various dimensions, thicknesses, and shapes [63]. Erb et al. mixed microparticles coated with superparamagnetic iron oxide nanoparticles into fluid polymer solutions that were gelled in the presence of a magnetic field. The resulting composites had microparticles aligned by the magnetic dipole axis. Composites containing 7.5 vol% of aligned microparticles had 250% higher swelling and 200% higher shrinkage in the direction perpendicular to the alignment axis. With microparticles aligned horizontally in a long thin gel rod, the rod thinned and lengthened when swelled with water [64].

Liu et al. also used magnetic fields to make a composite hydrogel with anisotropic mechanical properties. They made a positively-charged gel with negatively charged unilamellar titanate nanosheets embedded. Fabrication involved aligning the nanosheets in an aqueous colloidal dispersion with a magnetic field. The dispersion was then transformed into a composite hydrogel using light-triggered *in situ* polymerization. The resulting hydrogel behaves like white matter, deforming under shear forces applied along the direction of the embedded nanosheets, yet resisting compressive forces applied orthogonally. Shearing parallel to the nanostructures has a modulus of 0.6 kPa, while perpendicular shearing gave a modulus of 2.2 kPa. A higher perpendicular modulus means the material resists sideways squeeze. However the gel's shear anisotropy doesn't establish its tensile anisotropy, which is probably the mode where axon bundles fail [65].

Anisotropic hydrogels have been fabricated with light energy. Qin et al. mixed a water-soluble surface ligand into an aqueous solution with silver nanoparticles (NPs.) The ligands cleaved and bound to the silver NPs. Under UV radiation these ligand-silver nanocomposites aggregated into long 2D lamellar assemblies, only a single NP thick. These were put in polyacrylamide solution that formed dense, entangled cross-link chains with the lamellar assemblies. Qin et al. grew silver-nanoparticle lamellar assemblies under UV irradiation and entangled them in polyacrylamide. The resulting hydrogel could be stretched 20 times along the lamellar direction, twice that of perpendicular stretch [66].

While hydrogels can be tuned with compounds to mimic overall white matter mechanical behavior, another approach uses various materials that actually mimic white matter structure. Winter and colleagues did a series of studies that incorporated electrospun fiber mats, topographically similar to white matter tracts, in hydrogels to replicate features of parts of the occipital region responsible for vision. [67] The goal was to model tumor-migration rather than mechanics, though the authors propose that higher-aspect-ratio fibers would restrict flexibility along alignment directions and better mimic tract response to load [68]. Calhoun et al. found that the gray and white matter tissues differ in relaxation time, the duration needed to reduce internal stress after a sudden stretch or impact. White matter takes about three times as long to relax under a held strain. Its fibrous elements do not slide past one another as easily as the rounder gray matter elements[69]. The authors suggested that, in making a white matter surrogate material, increasing the aspect ratio and surface area of electrospun fibrous elements would limit their movement past one another, and restrict their flexible response to forces in the alignment directions. This could create a structural response to mechanical load similar to white matter.

Zhang et al. found a different method to align supramolecular fibrils over macroscopic scales. Isotropic solutions of peptide-containing molecules group into long filaments of bundled nanofibres under heating. By manually dragging these liquid crystals into salty media, they generated noodle-shaped viscoelastic gel strings that extended for centimeters. [70]

These studies of structure-mimicking gels report no mechanical data, and the gel fibers may have little mechanical strength. A very different hydrogel pathway was developed for connective (bone, tendon) and muscle tissue. These animal tissues have highly defined hierarchical structures that respond anisotropically to mechanical forces. Bai et al. tried to mimic the internal structure of such tissue by freeze casting poly N-isopropylacrylamide (monomer) and clay platelets together. The gels had micrometer-scale aligned porosity, nacre-like nanostructure, greater tensile strength along the alignment direction than across it, and, unusually for hydrogels, fracture energy in the range of cartilage. Anisotropic ice crystals grew along a temperature gradient and expelled the monomer and clay platelets from the freezing water, creating oriented voids. The composite was cryo-polymerized into a hydrogel, with highly aligned porous structure, and was stretchable, with greater tensile strength in mechanical impacts along their alignment direction than perpendicular impacts [71].

The white matter modulus at rest is different from its modulus during rotational acceleration. Indentation tests of bovine brains found that between a rate of 1 μm/s to 160 μm/s, white matter modulus increased from 1.26 kPa to 2.51 kPa. However 160 um/s is vastly slower than the result of a sports impact, by orders of magnitude (a typical ant walks 8300 μm/s.) [72] If modulus increases with acceleration rates, then white matter becomes very stiff during some impacts [73]. One way to directly

mimic this with hydrogels is through water loss, which increases their elastic modulus. The highest elastic modulus occurs in a nearly dry state [74].

Rate-dependent inversion likely explains much of the variance in published brain-property measurements that did not separate tissue types, and it sets a trap for surrogate design: a simulant tuned to match white matter at quasi-static rates will mismatch it at impact rates. A model brain used in an impact test may have a high elastic modulus in its resting state because it represents the brain during impacts. The modulus can be tuned to the head rotation velocity predictably caused by the mechanical instrument.

3.4 GUIDANCE: BRAIN MODELS WITH MATERIALS THAT MIMIC BRAIN MATTER

Between magnetic, light-templated, and freeze-cast routes, hydrogels can now be fabricated with a wide, tunable range of mechanical anisotropy at moduli overlapping white matter, using inexpensive materials and, in the magnetic case, a process that is consistent and shape-independent. This is the capability the silicone literature lacks.

Gray matter and white matter share brain volume somewhat equally, although with major shifts throughout the lifespan. Gray matter makes up the outermost layer of the brain, the cerebral cortex and the cerebellar cortex. It is also in the inner sections of the brain [75].

The architecture of brain matter is a significant factor in impact studies. The gray-white matter interface represents an area where mechanical mismatch of adjoining tissues occurs, and where there is the greatest risk of white matter damage. Soft and hard materials respond differently to mechanical stress, and mechanical instability occurs at their interface. The mismatched stress moduli can take a long distance (up to centimeters) to reach equilibrium, during which material damage occurs [76].

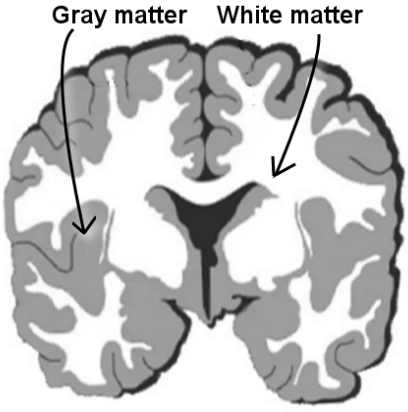


Figure 5 redrawn from Alkan, A. et al.

As brain tissue deforms under rotational acceleration, softer gray matter pulls the stiffer white matter along. This stiffness, while preventing axon deformation, imposes higher tensile stress on axons. Gray matter pulling the white matter causes greater tensile elongation of axons, compared to areas of white matter more isolated from gray matter [40].

A biomechanically realistic brain model for angular impact tests requires casting anisotropic hydrogels for white matter, and isotropic hydrogels or siloxanes for gray matter. These have to be cheek by jowl, with interfaces like real brains, so that impacts have realistic results. The molding

process must be fairly easy to perform and inexpensive, because model brains may be sacrificed in impact tests. Material should be recyclable and be quickly reformed.

The following is based on the author's process of prototype development of a model brain as described in the author's U.S. Patent 12,784,616 and the author's published international application WO2026042059 (see "Competing Interests" section.) This approach utilized axial scan slices from Subject 100206 in the Human Connectome Project database. The slices were processed to display four distinct brain tissue components: gray matter and white matter with three cardinal directions of anisotropy (anterior-posterior, left-right, and superior-inferior). Each axial slice measures approximately 1 mm in thickness and presents unique anatomical features. Importantly, gray and white matter images exhibit dimensional discrepancies and do not align precisely. Gray matter imaging is considered more anatomically accurate, while white matter imaging, which relies on water diffusion to assess axonal organization, is subject to greater geometric distortion. **Gray matter serves as the reference structure, to which directional-dependent (in each of the 3 cardinal directions) white matter is aligned and iteratively refined and averaged** to reinforce correct anatomical features. Casting molds were designed at 8 mm height (z-dimension), with each mold incorporating multiple axial slices. This scaling provides manageable physical models while preserving essential anatomical relationships. The single-subject source is deliberate: as Section 3.1 describes, the locations of peak axonal strain are consistent across individuals while magnitudes vary [34], so one subject's geometry can locate strain concentration, though it cannot predict magnitude in a particular individual. Alshareef et al. took the opposite route, an MRI template averaged from 20 volunteers [1]; averaging smooths the gray-white interface geometry at which strain concentrates.

White matter molds are filled with hydrogel precursors and a suspension of magnetic microparticles, platelets carrying a superparamagnetic iron oxide nanoparticle coating [64]. A magnetic field emitter is positioned to enforce directionality on the hydrogel, the dipole establishing one of three cardinal directions. **The gelation process produces a material with directional-dependent anisotropy.** Once cast, a sliding layer is removed, and the white matter falls in place into the negative area of the gray matter material. In this way, hydrogels with different anisotropic and isotropic directionalities can be configured together, as they are in a real brain.

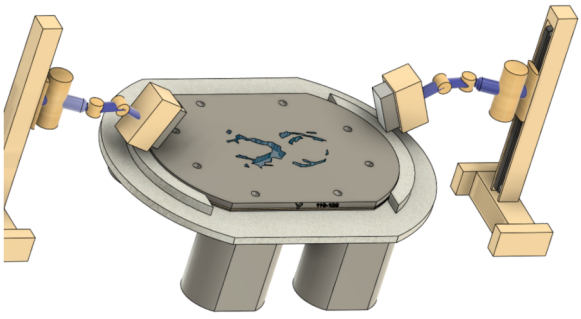


Figure 6

Bio-mimicking gels can be assembled by hand. Figure 6 shows a mold with magnetic microparticle-loaded liquid under a magnetic field during gelation. To form models in a reproducible and fast manner, a CAD program guiding servo driven injectors, or 3D printers, can be used. A single printer may alternate printing material and density during the printing process. Alternatively, material can be printed that serves as support for material later inserted in internal void [77].

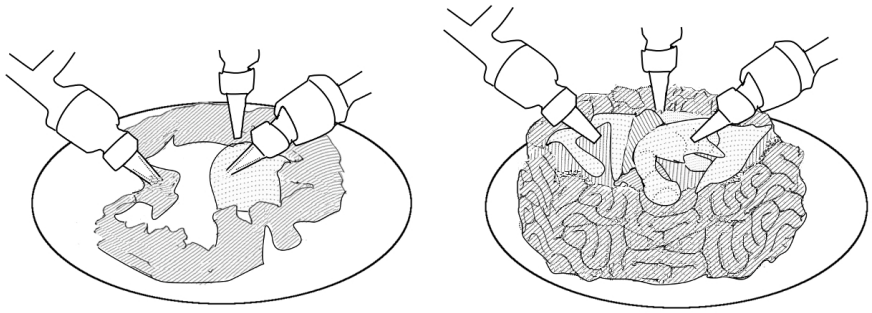


Figure 7

Figure 7 illustrates an automated system that uses servo motors to drive injectors to deposit white and gray matter simulant materials in place. Figure 8 illustrates a 3D printer and a robotic arm with an articulated arm that moves a "force" emitter, such as a magnetic force, to different positions. When the printer extrudes liquid or flexible white matter simulant material, the robotic arms moves into a position to apply the correct force to influence the white matter as its gels. This causes the hydrogel's anisotropy to accurately resemble the real brain component it serves to represent.

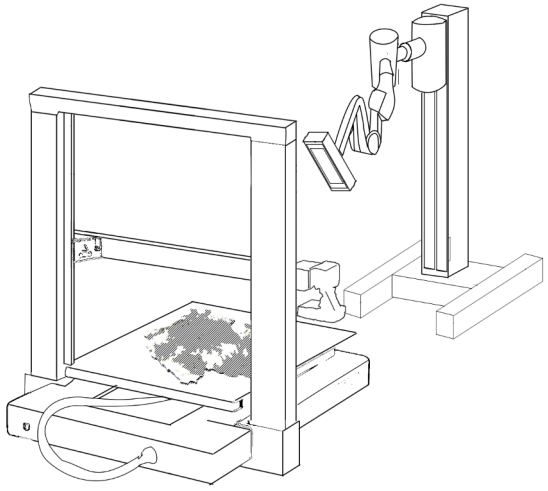


Figure 8

The model brain may have different materials cast simultaneously, in place. Polyvinyl alcohol (PVA) can be 3D printed as the mold. Because it is water soluble, PVA molds can be dissolved away, leaving behind the cast material. Different complex brain architectures can be 3D printed this way. White and

gray matter hydrogels or other materials are funneled, piped, or injected in mold components. Once the materials have taken shape, the PVA mold is dissolved [78].

4. THE SKULL

The skull's mechanical role in impact is defined by its composite construction, which no standard headform reproduces. This section reviews that construction, the surrogate skulls in current use, what is actually known about skull bone properties, including the substantial measurement disagreements a designer must navigate, printable materials that approximate those properties, and fabrication routes for a layered, biofidelic surrogate skull.

Skull bone is a three-layer composite. Two plates of cortical bone dense, with an organized microstructure conferring stiffness, stability and rigidity, sandwich a less dense layer of trabecular bone, called diploë in the skull, which is porous, spongy, and lightweight. Trabecular bone typically accounts for about 20% of total skull mass, though the fraction varies by location [79]. Lee et al. found a correlation of bending modulus and trabecular volume ratio. Their study examined skulls from cadavers, geriatric osseous tissues. Trabecular bone microstructure looks like very thin struts of a bridge. This distributes compressive forces through spaces between the struts filled with fluid and fat. These fillings, importantly for the cadaver literature below, do not survive death unchanged. The elastic modulus of two examined skulls varied from 1.7 to 2.7 GPa. Different skull bones in the same subject varied by as much as 1.3 GPa. Overall tensile strength varied from 42 to 53 MPa, with within individual strength varying up to 14 MPa [80].

The bones that encase the brain are cranial, while other skull bones are facial, forming the viscerocranium to support facial structures and house teeth. Cranial bones exist as separate structures because they cannot be fused for a baby to pass through a birth canal. After birth bones fuse, with the border areas called sutures. There are 22 cranial and facial bones of different shapes and thicknesses [81]. Figure 9 shows 5 cranial bones in the skull, including the overarching parietal and frontal bones [82].

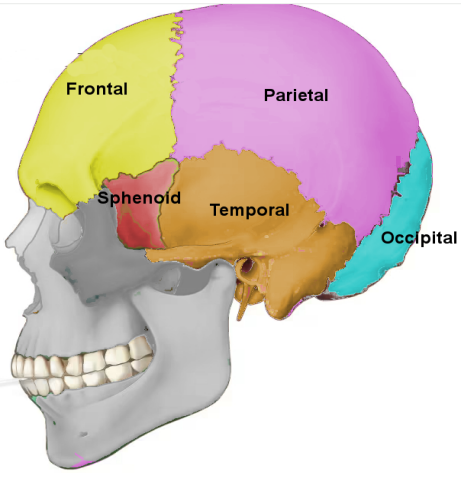


Figure 9 Redrawn from LoPresti [82]

The bone sandwich system provides outer stiffness to respond to sharp, sudden linear impacts. The diploe provides cushioning and shear strength, and by separating the cortical plates increases the bending strength of skull bones [83]. Thickness and density are the principal determinants of skull mechanical properties, and a strong positive correlation between thickness and stiffness is consistently observed.

A review found non-destructive impacts to the vertex region of the skull resulted in the stiffest bone response than similar impacts to the occipital, frontal, and parietal regions. At intermediate impact velocities (2.7–4.2 m/s) the parietal region was the stiffest. However evidence was too thin and methodologically heterogeneous to characterize region-specific skull response definitively. The impact response of commonly used surrogate heads is only calibrated for specific loading conditions (Hybrid III for frontal impacts, FOCUS for facial impacts, NOCSAE for helmeted impacts) and when used in alternative scenarios the response can be non-biofidelic. Hybrid III does not compare well to the cadaveric response in facial, vertex, or parietal impacts. Matching cadaver data is not a well-posed target, however, as cadaveric response varies from 40 to 5867 N/mm and cannot be reconciled across studies because of varying constraints and impactor geometry. A surrogate should aim to land within the physiological band reproduce structure rather than chase a single constant [84].

Standardized headforms, such as ISO/DIS 6220, use a urethane or metal head-like shell. The Hybrid III headform has a hollow aluminum shell and vinyl scalp (the scalp is less stiff than a human scalp to offset the aluminum stiffness.) A NOCSAE headform uses a polyethylene skull. A blast injury protection evaluation device (BIPED) developed by Defense Research and Development of Canada is the most elaborate. It has polyurethane skull material 6.35 mm thick, Sylgard 527 silicone as brain surrogate, water as cerebrospinal fluid, and tough urethane rubber skin [85]. A parametric study of the BIPED found skull thickness a significant variable in head acceleration across the impacts tested [86] Skull properties propagate measurably into the injury metrics these devices exist to record, and thus that skull biofidelity is not a cosmetic concern. None of these headforms is biofidelic in skull material, and none is layered.

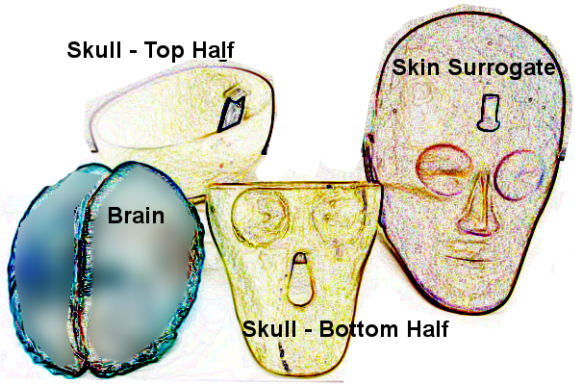


Figure 10 BIPED
redrawn from Ouellet & Philippens [85]

The elastic modulus of skull bones, which defines their resistance to deformation, is not consistent in published studies. Falland-Cheung et al. calculated the mean for six studies was 8.51 GPa, but varied from 1.23 to 15.54. The authors tested five skull simulant materials to assess their elastic moduli and flexural strength. The materials were epoxy resin, fibre filled epoxy resin, PETG, polylactic acid (PLA), and self-cure acrylic denture base resin. The elastic modulus of epoxy resin, 6.65 GPa, was closest to the mean 8.51. PLA flexural strength was closest to the mean for real bone, but its elastic modulus was less, 3.03 GPa. However given the variance in studies, this is not conclusive [87].

4.1 MODELING SKULLS WITH MULTIPLE MATERIALS

Since skull bones are combinations of trabecular and cortical, it may be important to determine the mechanics of each, and how they interact. Skull simulations may benefit from exploiting similar combinations, functionally straight-forward with 3D printing.

Trabecular skull bone elastic modulus varies by study, the difference in reported modulus of trabecular bone varies even more. Wu et al. examined 110 articles, and found assessment methods influence trabecular moduli results. Compression tests report elastic modulus around 10 GPa; ultrasonic test results are generally higher, in the teens, and nanoindentation is higher still, around 20 GPa. FE models report generally much lower elastic moduli, below 10 GPa. One study of trabecular elastic moduli in the same bones in 20 humans found a range of 2.7-9.1 GPa in mandibular condyle, the jaw's hinge bone. The same study found the T12 vertebra, near the base of the spine, varied between 8.5-15.6 GPa. None of Wu et al.'s studies examined skull trabecular and cortical bones separately [88].

Cortical bone mechanics may be location specific. Hunt et al. analyzed elastic modulus of cortical bone in femurs and tibias, of 19 individuals, using ultrasound. The mean tibia modulus was 34.11 GPa, the mean for femurs was 32.52 GPa. These were around 20% higher than some previous ultrasound results for cortical bone elastic modulus. Previous compression tests for cortical bones were around 20 GPa [89].

But cortical bone mechanics are different than trabecular bone. Rho et al. found that microspecimens of cortical bone measured ultrasonically 20.7 GPa (S.D. 1.9) and mechanically 18.6 GPa (S.D. 3.5). Average trabecular Young's modulus measured ultrasonically 14.8 GPa (S.D. 1.4) and mechanically 10.4 (S.D. 3.5). The authors concluded that when considered mechanically, cortical and trabecular bone are not the same material.

Studies find cortical bone modulus 1.5–2 times larger than trabecular in magnitude. Wang et al. tested trabecular and cortical bone moduli, using nanoindentation, in several rabbit skulls. Trabecular skull bones clustered around 10 GPa. Cortical bones in rabbit skulls had modulus around 17 GPa [90]. These are half the GPa reported for nanoindentation tests of non-skull trabecular bones in humans, but are larger than the elastic modulus reported for overall skull bones. However two materials in tight configuration with each other will combine for a different modulus. Table 3 collects the moduli reported in this section, tagged by level of measurement; values from different levels are not interchangeable.

TABLE 3. Reported skull-relevant elastic moduli and structural stiffness by level of measurement.

Level of measurement	**Specimen and method**	**Reported values**	**Ref.**
Whole-bone (intact cortical–diploë–cortical)	Human skull specimens, bending	Bending modulus 1.7–2.7 GPa; tensile strength 42–53 MPa	[80]
Whole-bone (across studies)	Six-study mean of elastic modulus	8.51 GPa (range 1.23–15.54 GPa)	[87]
Cortical tissue (long bones)	Human tibia and femur, ultrasound	32.5–34.1 GPa (~20 GPa by compression)	[89]
Trabecular tissue	Review; method-dependent	~10 GPa (compression); 10–20 GPa (ultrasound); ~20 GPa (nanoindentation); <10 GPa (FE models)	[88]
Skull cortical vs. trabecular	Rabbit skull, nanoindentation	Cortical ~17 GPa; trabecular ~10 GPa	[90]
Whole-head structural stiffness	Cadaver head compression (review)	40–5867 N/mm (force–deflection, not a modulus)	[84]

Material combinations are most studied in composites, usually with fibers embedded in a matrix. Their combination leads to modulus that may be anisotropic, with some load directions causing high modulus, and others low. Plywood-like fiber laminates, with many fiber directions crossing, obtain a isotropic higher modulus. However the cortical-trabecular sandwich is not a blend, but two materials layered. When materials with different elastic moduli are aligned over each other, the overall structure's flexibility can increase, and its elastic modulus decrease. Material with lower modulus, such as trabecular bone, absorbs and redistributes stresses to the more rigid cortical bone. This can reduce the elastic modulus of the overall structure [91].

PLA's ubiquity in 3D printing, ease of use, and mechanical proximity to several skull properties have made it the default research material, and the direct comparisons are encouraging. Mantecón et al. compared the flexural properties of 3D printed samples against Lee et al.'s cadaver results, at four different skull bone thicknesses. Bending strength of flat PLA specimens was between 92 and 123 MPa. Bending strength of skull bone was between 42 and 99 MPa. Bending modulus of PLA and skull bones differed for samples of the same thickness, except for PLA and skull bones 7.83 mm thick. The PLA modulus was between 1.81 and 2.71 GPa. The modulus of actual bone was between 1.7 and 3.95 GPa. The printed specimens were homogeneous, with no trabecular analog, yet the overall similarity is striking [92].

Similar mechanical result for PLA have been found in other studies. Zhao, Chen & Zhou tested PLA's elastic properties and tensile strength. Its elastic modulus varied between 2.5 and 2.8 GPa when printed flat. Its tensile strength was close to 50 MPa when printed flat. This latter measurement is squarely within Lee's 42–53 MPa skull tensile range. Thinner print layers raised both values [93]. PLA strength and elasticity modulus can be modified in several ways. Greater infill density increases strength and stiffness, as does increasing PLA crystallinity. Blending PLA with other polymers, such as masticated natural rubber, poly(ε-caprolactone), or poly(butylene adipate-co-terephthalate) (PBAT) can increase or decrease its flexibility and strength [94]. PLA/PBAT blends have much greater flexibility than PLA alone, but reduced tensile strength. PLA/PBAT blends further modified with organic clays (and gum or stearic acid rosins) recover most of the lost strength, without increasing elastic modulus. Adding organoclays (with gum or stearic-acid rosins) recovers most of the lost strength without raising elastic modulus. Different percentages of clay alter mechanical properties predictably [95, 96].

The tuning range brackets the cadaver data at both ends. Lee et al.'s results for one cadaver skull sample had a mean bending modulus of 1.7 GPa [80]. Ludwiczak, Frąckowiak & Leluk found that a PLA/PBAT combination with 5% clay had a 1.86 modulus. While the roughly linear clay–flexibility relation provides a path, through increasing clay percentage, to an exact 1.7 modulus match, unmodified PLA alone covers the mean skull bone bending modulus of 2.7 GPa of Lee's stiffer skull sample (2.7 GPa) [95].

A designer can thus hit any whole-bone modulus in the physiological band with one filament family.

4.2 GUIDANCE

Matching whole-bone constants with a homogeneous print may be sufficient for some tests, but the sandwich itself is printable, and reproducing it should recover skull-like dynamics, the distinct linear-impact stiffness and bending/shear behavior, rather than a single matched constant. Two approaches can accomplish this.

The density of any 3D material can be altered during printing, density-graded printing. Print density correlates with mechanical response, and infill can vary within a single print. **A skull printed as a thin dense outer surface, a sparse middle, and a thicker dense inner surface reproduces the cortical–diploë–cortical architecture in one material.** Different print densities correlate with different mechanical response, reproducing skull bone dynamics.

Alternatively, different materials could be assembled together. Some 3D printers have the capacity to switch materials on-the-fly. This allows both materials and print density to change, like actual skull bone internal structure. **Material switching can pair a stiffer cortical-layer filament with a more compliant diploë-layer material**, for instance PLA tables over a PLA/PBAT/clay core, letting both composition and density vary through the thickness, as in bone.

Printed skulls are generally produced in several parts and bonded, and the glue line is a known weak point. Hanna et al., testing adhesives for skull models under ballistic strain, found Pro-Flex 50, a 50 Shore A liquid polyurethane, the best performer. Bond lines might also be located along anatomical suture positions, where real skulls join, though whether sutures should be mechanically distinct in a surrogate is an open question the reviewed literature does not address.

5. CEREBROSPINAL FLUID

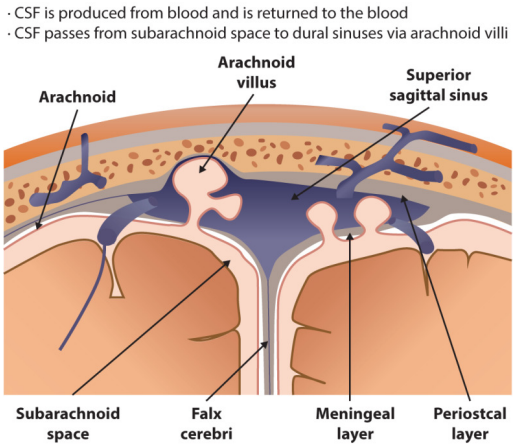


Fig. 11 CSF Circulation [99] reproduced under CC BY-NC-ND 4.0

Cerebrospinal fluid is the most consequential component that standard headforms omit. As the evidence below suggests, it is possibly the largest single lever on surrogate brain response. This section reviews the anatomy and mechanics a surrogate must approximate, the direct experimental evidence that a fluid layer transforms surrogate brain deformation, and a membrane-based fabrication approach.

CSF is a protective fluid that cushions the brain and spinal cord from mechanical injury. It is largely buoyant: full envelopment in CSF reduces the brain's effective weight from roughly 1,500 grams to about 50 grams. This near-neutral buoyancy proportionally reduces the forces the brain's own inertia generates during abrupt head movement. The CSF space is a dynamic pressure system that determines intracranial stress [97, 98].

The CSF protects the brain from fast and abrupt head movements. CSF occupies the subarachnoid space, between arachnoid and pia, not a simple annular gap but a compartment of complex geometry, crossed by arachnoid trabeculae and varying regionally in depth. The fluid is contained within the meninges, the three membranes surrounding the brain. From the brain surface outward: the pia mater, a delicate membrane averaging ~0.1 mm thick, adheres to the brain surface; it is the innermost layer of the meninges and is closest to the brain. Then comes arachnoid mater, ~0.2 mm thick; then the dura mater, ~1.1 mm thick, whose outermost surface attaches to the inner skull [99].. Two implications for modeling follow. First, the brain is coupled to the skull not only through fluid but through membrane, the dura to the skull, the pia to the brain. The "brain floats freely" motif is an approximation, and the tethering contributes the friction-like resistance to relative motion. Second, any surrogate CSF layer of uniform thickness is a simplification of a nonuniform space [100].

The clearest demonstration of CSF's mechanical significance in a physical model comes from Hanna et al. Their surrogate comprised an ABS skull and a homogeneous ballistic-gelatin brain, deliberately scaled down to leave a 2 mm gap between brain and inner skull. After sealing the assembly watertight,

they injected water into the area, as a proxy for CSF. They placed surrogate head models in a drop tower and compared frontal and crown impacts. The frontal orientation produced the most rotational motion and was used to test the model with CSF. The effect was large: the addition of a CSF layer reduced maximum shear strain 2.7-fold compared with a brain surrogate seated against the skull. Average strain rate was 6.8 times lower. The water layer caused the brain gel to experience less deformation. The fluid layer's influence on brain deformation exceeded that of the brain and skull material properties themselves. Two caveats attach to this result. The simplicity of the surrogate, a homogeneous gelatin brain and compliant ABS shell, may have amplified the fluid layer's relative influence, and a uniform 2 mm water annulus omits both the subarachnoid architecture and the dural attachment described above. The true effect in a more biofidelic assembly is therefore uncertain in magnitude. But the direction and rough scale of the finding align with the anatomical picture above: a near-buoyant brain simply cannot be loaded by skull motion the way a contact-coupled brain is [101].

5.1 GUIDANCE

Sealing an entire brain–skull assembly watertight, as Hanna et al. did, is exacting and failure-prone. It couples the fluid layer's integrity to every other joint in the model, including the glued skull seams. An alternative decouples the fluid system from the rest of the assembly: **fabricate a set of thin elastomeric membranes, each on the order of 1 mm thick, standing in for the meningeal layers, formed into a closed cavity between them, into which fluid (water, in the first instance) is injected.** The filled membrane assembly is then positioned between brain and skull, functioning as a self-contained, conformal fluid cushion.

This approach has several practical advantages. The fluid cell can be fabricated, filled, and leak-tested independently before assembly, and replaced without disturbing brain or skull. A punctured cell in a destructive test costs a membrane, not the model. Membrane thickness and stiffness offer a crude but real representation of the meninges' mechanical presence, which a bare water gap omits; the outer membrane seated against the skull loosely parallels the dural attachment. And the cavity's fill volume is adjustable, allowing the effective gap, and thus the degree of brain–skull coupling, to be varied parametrically, something Hanna's sealed 2 mm design could not do. The obvious extensions, regionally varying cavity depth to approximate subarachnoid geometry, a fluid of matched density and viscosity rather than plain water, membrane properties tuned to measured meningeal moduli, are refinements the basic architecture accommodates.

6. INSTRUMENTATION

A surrogate head is only as useful as what can be measured inside it, and instrumentation choice follows from the research question: pressure, deformation, or motion, and at what rate. The studies reviewed above already demonstrate the main options at work.

For internal pressure, embedded sensing is established practice: Zhu et al. recorded intracranial pressure in their Sylgard brain with an embedded fiber-optic sensor [46], an approach that scales naturally to arrays of multiple sensors at defined anatomical positions mapping pressure distribution across brain regions. This includes gray–white matter interfaces where injury risk is high. Fiber-optic sensors suit gel embedment because they are small, immune to electromagnetic interference, and mechanically unobtrusive; conventional pressure transducers serve at the skull wall.

For head kinematics, accelerometer arrays are standard. The HITS helmet system 2 is the field-deployed example [19]. Skull-mounted triaxial accelerometers capture linear acceleration and gyroscopes capture instantaneous angular velocity. These instruments, however, report instantaneous quantities, from which total rotational excursion must be reconstructed by integration, with attendant drift. For rotation-dominated testing, which is the loading mode this review's surrogate is designed for, the author has developed and patented [102] a complementary sensor that measures rotational displacement directly: a Hall-effect sensor reading a magnetic array distributed on an adjacent surface, such that the sensor's traversal of the array yields the distance and velocity of head rotation over the impact event, eliminating the integration step and its accumulated error.

For internal deformation, the quantity most directly tied to injury mechanisms, strain can be measured by embedded gauges, but the material choices of this review offer a better route: hydrogels are optically transparent, so marker particles embedded at casting can be tracked through the gel by high-speed camera, and digital image correlation converts marker fields into full strain maps. Hanna et al.'s shear-strain and strain-rate comparisons [101], rest on exactly this kind of measurement. Transparency is thus a further advantage of hydrogel brains over opaque alternatives: the surrogate's interior is visible. Distributed combinations, such as pressure arrays, kinematic sensors, and optical strain fields, synchronized and sampled at rates sufficient for millisecond-scale events, yield three-dimensional maps of the quantities that injury models actually predict, and the validation data that this review calls for.

7. CONCLUSIONS

Physical head surrogates remain indispensable for TBI research, they capture responses, particularly rotational, that head instrumentation, cadaver tests, animal studies, and finite element models cannot yet simulate, but the standard headforms were never designed for biofidelity. This review has argued that materials and fabrication methods now exist to close the gap at each anatomical level, and at costs low enough that surrogate components can be treated as consumable.

7.1 NECK

For the neck, the evidence converges on anticipation as the decisive variable. Muscle activation, triggered largely by visual awareness of an incoming impact, measurably reduces rotational head

acceleration; impacts arriving from peripheral or unseen directions meet a less-defended neck. Actively mimicking musculature in a surrogate is impractical with current materials. Existing neck models like Hybrid III and Thor use simplified materials (metal discs with rubber) that don't accurately represent human muscle behavior. Instead, the functional consequence of muscle activation can be engineered directly. **Neck stiffness should be configurable by test scenario: stiffer for impacts modeled as arising within the visual field, more flexible as the modeled impact direction moves into peripheral vision or beyond the periphery.** Existing hardware permits versions of this adjustment; purpose-built neckforms could make it systematic.

7.2 BRAIN

For the brain, the central biofidelic requirement concerns material heterogeneity. The two distinct types of brain tissue respond differently to impacts. White matter deforms anisotropically along axonal tract directions. This is the best available predictor of mild TBI. Gray matter responds isotropically. Injury concentrates where gray and white matter meet, as each responds differently to mechanical loads, causing mechanical mismatch. The silicone simulants standard in blast research match brain stiffness but are categorically isotropic, unrealistic for white matter. Anisotropic hydrogels emerging from biomedical materials research align mechanical behavior magnetically, electrically, by shear, by light-templated assembly, or by freeze casting. They can exhibit directional mechanics similar to white matter at appropriate moduli. **A biofidelic surrogate brain therefore combines anisotropic hydrogel white matter with isotropic hydrogel or ultrasoft siloxane gray matter, assembled with anatomically realistic interfaces, ensuring white and gray matter interfaces are accurate.**

7.3 SKULL

For the skull, the design target is the skull’s cortical–diploë–cortical sandwich, two dense cortical bone layers surrounding spongy trabecular bone (diploe). This provides both rigidity and shock absorption. Whole-bone moduli, resulting from intact specimens tested with their full three-layer structure, as distinct from the moduli of cortical or trabecular tissue measured in isolation, are roughly 1.7–2.7 GPa, well below either component's modulus. PLA and PLA/PBAT–clay blends cover this whole-bone moduli with a single tunable filament family, but the elastic modulus of different skull bones varies widely (1.7-15.5 GPa). Short carbon fiber composites reach 2–15 GPa, and continuous carbon fiber PLA 15–26 GPa. **Using graded-density or multi-material printing, a sandwich architecture combining higher moduli components is reproduced.** A layered print with a compliant core will have an effective through-thickness modulus below its stiffest constituent, because the soft layer absorbs and redistributes stress, as real bones do. Reduced infill density does the same thing within a single material. Sparse infill is, mechanically, a compliant core. **Both sandwich routes can reproduce a**

skull, as high moduli in component structures combine in a whole structure with a low GPa. This will enhance biomechanical accuracy.

7.4 CEREBROSPINAL FLUID

For cerebrospinal fluid, the evidence indicates a first-order effect rather than a refinement. CSF cushions the brain during impact, its buoyancy and the fluid gap it maintains substantially reduce the rotational and shear strain transmitted to brain tissue. It is held in place by the three meningeal membranes: the pia, arachnoid, and dura. The one direct surrogate test bears this out: when a head model enclosed its artificial brain in a fluid layer standing in for CSF, brain deformation fell severalfold, an influence exceeding that of the brain and skull materials themselves. **Rather than sealing an entire brain and skull assembly watertight, and flooding the gap between them with water, the practical implementation is a set of thin membranes forming a sealed, fluid-filled cavity seated against the inner skull.** This membrane-bounded fluid cell loosely parallels the meninges it stands in for, and it is independently fillable, leak-testable, and replaceable. This is more practical than a whole-model seal, and a step closer to the layered anatomy that actually contains CSF.

7.5 THE INTEGRATED SURROGATE

Assembled together, these components describe a head surrogate that is substantially more biofidelic than current simplified models in precisely the properties that govern rotational injury, the loading mode dominant in sports collisions and vehicle accidents, and the one existing headforms represent worst. The design combines anisotropic hydrogels for white matter with isotropic hydrogels or ultrasoft siloxanes for gray matter, joined at anatomically realistic interfaces, since the gray–white boundary is where mechanical mismatch concentrates strain and injury localizes. Around this composite brain sits a membrane-bounded fluid layer standing in for cerebrospinal fluid, within a printed skull surrogate tuned, by blend, fiber reinforcement, or layered sandwich construction, to skull bone response. The whole rests on a neck whose stiffness is configured to the modeled impact direction relative to the visual field, reproducing the protective difference between anticipated and unseen impacts. Each element is inexpensive, most are printable, and several are recyclable, so that surrogate components can be treated as consumable in destructive testing. No single element is speculative; each rests on demonstrated materials and methods reviewed above. What remains is their integration and validation, under matched loading conditions, which is the program of work this review is intended to enable.

COMPETING INTERESTS

The author was awarded U.S. Patent 12,784,616 for biomechanically realistic brain models. The author

filed an international application for biomechanically realistic brain models at WIPO, PCT/IB2025/062404, published at patentscope.wipo.int (WO2026042059). The author was previously awarded U.S. patents 11,464,270 and 12,433,362 for helmet systems that reduce rotational acceleration under tangential impacts. The author has refined the helmet system in response to prototype testing, in U.S. patent application No. 19/757,298 (pending). The author was awarded U.S. patent 12,702,180 for a magnetic sensor that measures rotational and tangential motion of a helmet. The author filed U.S. patent application No. 19/291,259 (allowed) for a helmet system that triggers an airbag to rapidly inflate around a player's neck when impact thresholds are exceeded.

REFERENCES

1. Alshareef, A. A., et al. Multimodal characterization of intracranial biomechanics in a 3D biofidelic head surrogate. J. Mech. Behav. Biomed. Mater. 173:107250, 2026.

2. Coyle, B. M., inventor. Model brain. U.S. Patent 12,784,616, issued Nov. 3 2026.

3. Walsh, E. S., M. Kendall, A. Post, et al. Comparative analysis of Hybrid III neckform and an unbiased neckform. Sports Eng. 21:479–485, 2018.

4. Humm, J., and N. Yoganandan. Lower neck injury assessment risk curves based on matched-pair human data for anthropomorphic test devices. Mil. Med. 186(Suppl 1):639–644, 2021.

5. Wang, Z. J., et al. Neck biofidelity comparison of THOR-AV, THOR and Hybrid III 50th dummies. Proc. IRCOBI Conf. 2021:136–156, 2022.

6. Awad, N., W. W. El-Dakhakhni, and A. A. Gilani. A physical head and neck surrogate model to investigate blast-induced mild traumatic brain injury. Arab. J. Sci. Eng. 40:945–958, 2015.

7. Bogduk, N., and S. Mercer. Biomechanics of the cervical spine. I: Normal kinematics. Clin. Biomech. 15(9):633–648, 2000.

8. Swartz, E. E., R. T. Floyd, and M. Cendoma. Cervical spine functional anatomy and the biomechanics of injury due to compressive loading. J. Athl. Train. 40(3):155–161, 2005.

9. Yang, H., et al. Effective modulus of the human intervertebral disc and its effect on vertebral bone stress. J. Biomech. 49(7):1134–1140, 2016.

10. Arnold, N., J. Scott, and T. R. Bush. A review of the characterizations of soft tissues used in human body modeling: scope, limitations, and the path forward. J. Tissue Viability 32(2):286–304, 2023.

11. Begley, A. Houdini: The Elusive American. New Haven: Yale University Press, 2020.

12. Nightingale, R. W., et al. Impact responses of the cervical spine: a computational study of the effects of muscle activity, torso constraint, and pre-flexion. J. Biomech. 49(4):558–564, 2016.

13. Nasim, M., and U. Galvanetto. Muscle activity on head-first compression responses of a finite element neck model. Forces Mech. 10:100163, 2023.

14. Mansell, J., et al. Resistance training and head-neck segment dynamic stabilization in male and female collegiate soccer players. J. Athl. Train. 40(4):310–319, 2005.

15. Ito, Y., et al. The functional effectiveness of neck muscle reflexes for head-righting in response to sudden fall. Exp. Brain Res. 117:266–272, 1997.

16. Bauer, J. A., et al. Impact forces and neck muscle activity in heading by collegiate female soccer players. J. Sports Sci. 19:171–179, 2001.

17. Kumar, S., Y. Narayan, and T. Amell. Role of awareness in head-neck acceleration in low velocity rear-end impacts. Accid. Anal. Prev. 32:233–241, 2000.

18. Tierney, R. T., et al. Gender differences in head-neck segment dynamic stabilization during head acceleration. Med. Sci. Sports Exerc. 37(2):272–279, 2005.

19. Mihalik, J. P., et al. Collision type and player anticipation affect head impact severity among youth ice hockey players. Pediatrics 125(6):e1394–e1401, 2010.

20. Sanders, O. P., et al. Protective balance and startle responses to sudden freefall in standing humans. Neurosci. Lett. 586:8–12, 2015.

21. Schmidt, J. D., et al. Head impact magnitude in American high school football. Pediatrics 138(2):e20154231, 2016.

22. Bexander, C. S. M., and P. W. Hodges. Cervical rotator muscle activity with eye movement at different speeds is distorted in whiplash. PM R 11(9):944–953, 2019.

23. Rungta, S., et al. Preparatory activity links the frontal eye field response with small amplitude motor unit recruitment of neck muscles during gaze planning. J. Neurophysiol. 126(2):451–463, 2021.

24. Cholewicki, J., M. M. Panjabi, and A. Khachatryan. Stabilizing function of trunk flexor-extensor muscles around a neutral spine posture. Spine 22:2207–2212, 1997.

25. Stevenson, R. A., et al. Interactions between the spatial and temporal stimulus factors that influence multisensory integration in human performance. Exp. Brain Res. 219(1):121–137, 2012.

26. Younis, O., et al. A hazard detection and tracking system for people with peripheral vision loss using smart glasses and augmented reality. Int. J. Adv. Comput. Sci. Appl. 10(2):1–9, 2019.

27. Miller, R. A., et al. Effects of protective American football headgear on peripheral vision reaction time and visual target detection in Division I NCAA football players. Sports (Basel) 7(9):231–238, 2019.

28. Kiefer, A. W., et al. Less efficient oculomotor performance is associated with increased incidence of head impacts in high school ice hockey. J. Sci. Med. Sport 21(1):4–9, 2018.

29. Clark, J. F., et al. Lack of eye discipline during headers in high school girls soccer: a possible mechanism for increased concussion rates. Med. Hypotheses 100:10–14, 2017.

30. Carlsen, R. W., et al. A quantitative relationship between rotational head kinematics and brain tissue strain from a 2-D parametric finite element analysis. Brain Multiphys. 2:100024, 2021.

31. Giordano, C., et al. The influence of anisotropy on brain injury prediction. J. Biomech. 47:1052–1059, 2014.

32. Giordano, C., and S. Kleiven. Evaluation of axonal strain as a predictor for mild traumatic brain injuries using finite element modeling. Stapp Car Crash J. 58:29–62, 2014.

33. Veenith, T., et al. Inter subject variability and reproducibility of diffusion tensor imaging within and between different imaging sessions. PLoS ONE 8(6):e65941, 2013.

34. Giordano, C., S. Zappalà, and S. Kleiven. Anisotropic finite element models for brain injury prediction: the sensitivity of axonal strain to white matter tract inter-subject variability. Biomech. Model. Mechanobiol. 16(4):1269–1293, 2017.

35. Zikopoulos, B., M. Á. García-Cabezas, and H. Barbas. Parallel trends in cortical gray and white matter architecture and connections in primates allow fine study of pathways in humans and reveal network disruptions in autism. PLOS Biol. 16(2):e2004559, 2018.

36. Barbas, H., and N. Rempel-Clower. Cortical structure predicts the pattern of corticocortical connections. Cereb. Cortex 7(7):635–646, 1997.

37. Smith, S., et al. Structural variability in the human brain reflects fine-grained functional architecture at the population level. J. Neurosci. 39(31):6136–6149, 2019.

38. Nazeri, A., et al. In vivo imaging of gray matter microstructure in major psychiatric disorders: opportunities for clinical translation. Biol. Psychiatry Cogn. Neurosci. Neuroimaging 5(9):855–864, 2020.

39. Pribe, J. D., T. Siegmund, and J. J. Kruzic. The roles of yield strength mismatch, interface strength, and plastic strain gradients in fatigue crack growth across interfaces. Eng. Fract. Mech. 235:107072, 2020.

40. Alisafaei, F., et al. Mechanisms of local stress amplification in axons near the gray-white matter interface. Biophys. J. 119(7):1290–1300, 2020.

41. Bayly, P. V., et al. Deformation of the human brain induced by mild acceleration. J. Neurotrauma 22(8):845–856, 2005.

42. Giordano, C., and S. Kleiven. Connecting fractional anisotropy from medical images with mechanical anisotropy of a hyperviscoelastic fibre-reinforced constitutive model for brain tissue. J. R. Soc. Interface 11(91):20130914, 2014.

43. Chan, D. D., et al. Statistical characterization of human brain deformation during mild angular acceleration measured in vivo by tagged magnetic resonance imaging. J. Biomech. Eng. 140(10):101005, 2018.

44. Hossain, S. G. M. Material modeling and analysis for the development of a realistic blast headform. M.S. thesis, University of Nebraska–Lincoln, Lincoln, NE, 2010.

45. Zhang, J. Blast-induced tinnitus: animal models. J. Acoust. Soc. Am. 146(5):3811–3831, 2019.

46. Zhu, F., C. Wagner, A. Dal Cengio Leonardi, X. Jin, P. VandeVord, C. Chou, K. H. Yang, and A. I. King. Using a gel/plastic surrogate to study the biomechanical response of the head under air shock loading: a combined experimental and numerical investigation. Biomech. Model. Mechanobiol. 11:341 –353, 2012.

47. Darvish, K. K., and J. R. Crandall. Nonlinear viscoelastic effects in oscillatory shear deformation of brain tissue. Med. Eng. Phys. 23(9):633–645, 2001.

48. Nicolle, S., M. Lounis, R. Willinger, and J. F. Palierne. Shear linear behavior of brain tissue over a large range of frequencies. Biorheology 42(3):209–223, 2005.

49. Hrapko, M., et al. Characterisation of the mechanical behaviour of brain tissue in compression and shear. Biorheology 45(6):663–676, 2008.

50. Singh, G., P. Yadav, and A. Chanda. Development of biofidelic skin simulants based on fresh cadaveric skin tests. Eur. Burn J. 5(4):454–463, 2024.

51. Chanda, A., et al. Biofidelic human brain tissue surrogates. Mech. Adv. Mater. Struct. 25(15–16):1335–1341, 2018.

52. Yang, W., et al. On the tear resistance of skin. Nat. Commun. 6:6649, 2015.

53. Chanda, A., V. Unnikrishnan, and Z. Flynn. Biofidelic skin simulant. U.S. Patent 10,954,383, filed March 3, 2018, issued March 23, 2021.

54. Budday, S., et al. Fifty shades of brain: a review on the mechanical testing and modeling of brain tissue. Arch. Comput. Methods Eng. 27:1187–1230, 2020.

55. Vatankhah-Varnosfaderani, M., et al. Chameleon-like elastomers with molecularly encoded strain-adaptive stiffening and coloration. Science 359(6383):1509–1513, 2018.

56. Ray, L. A., et al. MRI-to-synthetic 3D gel brain: proof-of-concept fabrication for intra-parenchymal diffusion studies. bioRxiv, 2022. doi: 10.1101/2022.10.27.514134.

57. Wang, J., et al. Hydrogels with brain tissue-like mechanical properties in complex environments. Mater. Des. 234:112338, 2023.

58. Cacopardo, L., et al. Engineering hydrogel viscoelasticity. J. Mech. Behav. Biomed. Mater. 89:162–167, 2019.

59. Kainz, M. P., et al. Poro-viscoelastic material parameter identification of brain tissue-mimicking hydrogels. Front. Bioeng. Biotechnol. 11:1143304, 2023.

60. Alexander, G., et al. Model-driven exploration of poro-viscoelasticity in human brain tissue: be careful with the parameters! Interface Focus 14:20240026, 2024.

61. Fan, H., and J. P. Gong. Fabrication of bioinspired hydrogels: challenges and opportunities. Macromolecules 53:2769–2782, 2020.

62. Bercea, M. Bioinspired hydrogels as platforms for life-science applications: challenges and opportunities. Polymers (Basel) 14(12):2365, 2022.

63. Sano, K., Y. Ishida, and T. Aida. Synthesis of anisotropic hydrogels and their applications. Angew. Chem. Int. Ed. 57:2532–2543, 2018.

64. Erb, R. M., et al. Self-shaping composites with programmable bioinspired microstructures. Nat. Commun. 4:1712, 2013.

65. Liu, M., et al. An anisotropic hydrogel with electrostatic repulsion between cofacially aligned nanosheets. Nature 517:68–72, 2015.

66. Qin, H., et al. Anisotropic and self-healing hydrogels with multi-responsive actuating capability. Nat. Commun. 10:2202, 2019.

67. Rao, S. S., et al. Glioblastoma behaviors in three-dimensional collagen-hyaluronan composite hydrogels. ACS Appl. Mater. Interfaces 5(19):9276–9284, 2013.

68. Rao, S. S., et al. Mimicking white matter tract topography using core-shell electrospun nanofibers to examine migration of malignant brain tumors. Biomaterials 34(21):5181–5190, 2013.

69. Calhoun, M. A., et al. Beyond linear elastic modulus: viscoelastic models for brain and brain mimetic hydrogels. ACS Biomater. Sci. Eng. 5(8):3964–3973, 2019.

70. Zhang, S., et al. A self-assembly pathway to aligned monodomain gels. Nat. Mater. 9(7):594–601, 2010.

71. Bai, H., et al. Thermoresponsive composite hydrogels with aligned macroporous structure by ice-templated assembly. Chem. Mater. 25(22):4551–4556, 2013.

72. Budday, S., R. Nay, and E. Kuhl, et al. Mechanical properties of gray and white matter brain tissue by indentation. J. Mech. Behav. Biomed. Mater. 46:318–330, 2015.

73. Moss, W. C., M. J. King, and E. G. Blackman. Skull flexure from blast waves: a mechanism for brain injury with implications for helmet design. Phys. Rev. Lett. 103:108702, 2009.

74. Li, Z., et al. The effect of water content on the elastic modulus and fracture energy of hydrogel. Extreme Mech. Lett. 35:100617, 2019.

75. Narvacan, K., et al. Evolution of deep gray matter volume across the human lifespan. Hum. Brain Mapp. 38(8):3771–3790, 2017.

76. Fang, Y., et al. Dissecting biological and synthetic soft-hard interfaces for tissue-like systems. Chem. Rev. 122(5):5233–5276, 2022.

77. Lima, T. d. P. L., et al. 3D bioprinting technology and hydrogels used in the process. J. Funct. Biomater. 13(4):214, 2022.

78. Brooks-Richards, T. L., et al. Dissolvable 3D printed PVA moulds for melt electrowriting tubular scaffolds with patient-specific geometry. Mater. Des. 215:110466, 2022.

79. Osterhoff, G., et al. Bone mechanical properties and changes with osteoporosis. Injury 47(Suppl 2):S11–S20, 2016.

80. Lee, J. H. C., et al. An investigation on the correlation between the mechanical properties of human skull bone, its geometry, microarchitectural properties, and water content. J. Healthc. Eng. 2019:6515797, 2019.

81. Henwood, B. J., and G. Appleby-Thomas. The suitability of Synbone® as a tissue analogue in ballistic impacts. J. Mater. Sci. 55(7):3022–3033, 2020.

82. LoPresti, L. Head and Neck Anatomy: Part I – Bony Structures. dentalcare.com continuing-education course CE591, 2025.

83. Zapata, U., and Q. Wang. Material properties of the skull layers of the primate parietal bone: a single-subject study. PLoS ONE 15(3):e0229244, 2020.

84. Thompson-Bagshaw, D. W., R. D. Quarrington, and C. F. Jones. A review of the compressive stiffness of the human head. Ann. Biomed. Eng. 50:1750–1761, 2022.

85. Ouellet, S., and M. Philippens. The multi-modal responses of a physical head model subjected to various blast exposure conditions. Shock Waves 28:19–26, 2017.

86. Azar, A., et al. Protective headgear attenuates forces on the inner table and pressure in the brain parenchyma during blast and impact. J. Biomech. Eng. 142(4):041009, 2020.

87. Falland-Cheung, L., et al. Investigation of the elastic modulus, tensile and flexural strength of five skull simulant materials for impact testing of a forensic skin/skull/brain model. J. Mech. Behav. Biomed. Mater. 68:303–307, 2017.

88. Wu, D., et al. Young's modulus of trabecular bone at the tissue level: a review. Acta Biomater. 78:1 –12, 2018.

89. Hunt, K. D., et al. Ultrasonic determination of the elastic modulus of human cortical bone. Med. Biol. Eng. Comput. 36:51–56, 1998.

90. Wang, L., et al. Regional variation of the cortical and trabecular bone material properties in the rabbit skull. PLoS ONE 19(2):e0298621, 2024.

91. Ashby, M. F., and D. R. H. Jones. Properties of composites and foams. In: Engineering Materials 2. 4th ed. Oxford: Butterworth-Heinemann, 2013, pp. 477–492.

92. Mantecón, R., et al. Additive manufacturing and mechanical characterization of PLA-based skull surrogates. Polymers 15(1):58, 2022.

93. Zhao, Y., Y. Chen, and Y. Zhou. Novel mechanical models of tensile strength and elastic property of FDM AM PLA materials: experimental and theoretical analyses. Mater. Des. 181:108089, 2019.

94. Huang, Y., et al. A new strategy to improve viscoelasticity, crystallization and mechanical properties of polylactide. Polym. Test. 97:107160, 2021.

95. Ludwiczak, J., S. Frąckowiak, and K. Leluk. Study of thermal, mechanical and barrier properties of biodegradable PLA/PBAT films with highly oriented MMT. Materials (Basel) 14(23):7189, 2021.

96. Moustafa, H., et al. PLA/PBAT bionanocomposites with antimicrobial natural rosin for green packaging. ACS Appl. Mater. Interfaces 9(23):20132–20141, 2017.

97. Adigun, O. O., and M. A. Al-Dhahir. Anatomy, head and neck, cerebrospinal fluid. In: StatPearls [Internet]. Treasure Island, FL: StatPearls Publishing, 2021.

98. Sakka, L., G. Coll, and J. Chazal. Anatomy and physiology of cerebrospinal fluid. Eur. Ann. Otorhinolaryngol. Head Neck Dis. 128(6):309–316, 2011.

99. Tumani, H., A. Huss, and F. Bachhuber. The cerebrospinal fluid and barriers – anatomic and physiologic considerations. Handb. Clin. Neurol. 146:21–32, 2018.

100. Sehgal, I., and J. M. Das. Anatomy, back, spinal meninges. In: StatPearls [Internet]. Treasure Island, FL: StatPearls Publishing, updated 2023.

101. Hanna, M., et al. Anatomical features and material properties of human surrogate head models affect spatial and temporal brain motion under blunt impact. Bioengineering (Basel) 11(7):650, 2024.

102. Coyle, B. M., inventor. Helmet rotation damping with negative torque. U.S. Patent 12,702,180, issued August 11, 2026.